

Computational Structure Activity Relationship Studies on the CD1d/Glycolipid/TCR Complex Using AMBER and AUTODOCK

Janos Nadas,^{*,†,‡} Chenglong Li,[§] and Peng George Wang^{†,‡}

Departments of Chemistry and Biochemistry and Division of Medicinal Chemistry, College of Pharmacy, The Ohio State University, Columbus, Ohio 43210

Received August 5, 2008

The human CD1d protein presents a wide range of lipids to the TCR of invariant natural killer T cells (iNKT). α -GalCer is one of the most potent iNKT stimulatory ligands presented by CD1d. The lipid portion of this ligand has been extensively investigated over the course of the past few years; however, the sugar portion of the ligand has received minimal attention. The following research focuses on computationally analyzing the recently crystallized CD1d/ α -GalCer/TCR tertiary complex by molecular dynamics simulations using AMBER along with studying the structure activity relationship of the sugar headgroup also by simulation and docking using Autodock for a variety of α -GalCer analogs. The results show that the crystal structure is stable under simulation making it an accurate representation of the CD1d/ α -GalCer/TCR complex and that modifications to the C2' and C3' positions of the sugar are not tolerated by the tertiary complex, whereas modifications to the C4' position are tolerated.

INTRODUCTION

In contrast to the conventional major histocompatibility complexes (MHC) presenting peptides to the CD4⁺ and CD8⁺ T cells of the immune system,^{1–3} MHC-I-like CD1 glycoproteins present lipids and glycolipid antigens to non-MHC-restricted T lymphocytes.^{4,5} There are five classes of CD1 proteins in humans based on sequence homology, comprised of group I CD1 (CD1a, -b, -c) and group II CD1 (CD1d and CD1e).^{6–10} Though in mice, there is only a single class of CD1d protein (mCD1d) which is homologous to the human isoform CD1d.¹¹ The highly conserved human isoform CD1d presents a wide range of lipids to invariant natural killer T (iNKT) cells, which coexpress the natural killer marker NK1.1 and T cell receptor (TCR).¹² These iNKT cells express the invariant V α 24-J α 18 chains paired with V β 11 chains which have been shown to be involved in antigen recognition.^{6,13,14}

α -Galactosylceramide (α -GalCer), a glycosphingolipid, was originally discovered by the Pharmaceutical Division of the Kirin Brewery Company during a screen for reagents derived from the marine sponge *Agelas mauritianus* that prevent tumor metastases in mice.^{15,16} The α -GalCers are branched galactosylceramides with an uncommon α linkage between the sugar and ceramide. Structure activity relationship (SAR) studies of the glycosphingolipids produced an optimized ligand for CD1d binding, termed KRN7000 (from now on referred to as α -GalCer), which has an 18-carbon sphingosine and a 26-carbon acyl chain.^{17,18} α -GalCer can be readily loaded onto CD1d, and on the surface of antigen presenting cells the CD1d/ α -GalCer complex can be recognized by the TCR of all types of iNKT cells.^{19–21} The CD1d/

α -GalCer/TCR association triggers a rapid, transient, and massive response of iNKT cells that accumulates Th1 and Th2 cytokines and initiates the following immunological cascades.

A variety of α -GalCer analogs have since been synthesized in search of improved biological activities.^{22–27} The results showed that the structures of sphingosines and acyl chains affect not only the magnitude of the iNKT cell stimulation but also the profile of the stimulation.^{23,24} For example, the analog OCH, a shortened fully saturated lipid, was found to induce a T_H2-biased cytokine release that also changed the IFN- γ production by the iNKT cells.²⁸ Much less investigation has been done on how the sugar moiety of the glycolipid participates in the stimulation of iNKT cells. The replacement of the galactose sugar with glucose, where the 4'-OH is equatorial rather than axial, resulted in a weaker agonist than α -GalCer.²⁹ The 2'-OH of the sugar was found to be very critical for CD1d binding.^{30,31} When it was substituted by hydrogen, fluoro, acetyl amide or axial OH (mannose), the biological activities of the resulting analogs were dramatically decreased.^{32,33} Incorporation of a fluorophore or biotin group at C6' of the galactose of α -GalCer did not cause significant stimulatory differences compared to α -GalCer,³⁴ which suggested that small modifications at C6' position of the galactose did not interfere with the stimulatory potency of the glycolipid. These discoveries were in agreement with the experiments done by the laboratories of Taniguchi,²⁹ Kronenberg,³⁵ and Bendelac.³⁶ When the C2', C3', or C4' of the galactose was capped with another sugar, the resulting diglycosylceramide lost its activity if the additional sugar cap was not removed by a glycosidase. In contrast, the Gal α 1,6Gal α Cer still stimulated iNKT cells without truncation to the monoglycosylceramide. All these results demonstrated that even relatively minor changes in glycolipid structure, either on sugar moiety or lipid moiety, can result in large affinity differences among the binding partners.

* Corresponding author e-mail: nadas.2@osu.edu.

† Department of Chemistry.

‡ Department of Biochemistry.

§ Division of Medicinal Chemistry, College of Pharmacy.

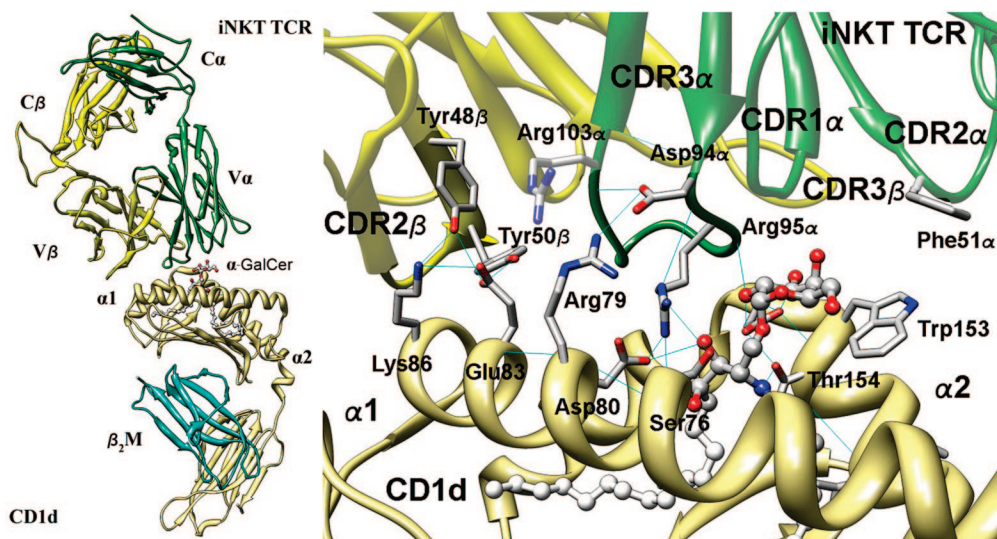


Figure 1. The binding orientation of the CD1d/α-GalCer/TCR complex is shown along with the hydrogen bonding network between the two proteins and those with the glycolipid. CDR α loops are green and CDR β are yellow.

Over the course of several years, the only structural data available were the binary crystal structures of CD1d with ligands α-GalCer,³⁷ PBS-25,²⁸ sulfatide,²⁸ GalA-GSL,³⁸ and most recently iGb3.³⁹ The binary complex interaction with TCR was widely believed to resemble the binding footprint of the related pMHC/peptide/TCR footprint where the two proteins would adopt a perpendicular orientation relative to each other. The crystallization of lone TCR proteins led two groups, Gadola et al.⁴⁰ and Kjer-Nielsen et al.,⁴¹ to create theoretical models of the CD1d/glycolipid/TCR ternary complex based on this assumption that the CD1d ternary complex would look similar to the pMHC ternary complex. However, the very recent successful crystallization of the ternary complex CD1d/α-GalCer/TCR by Rossjohn et al.⁴² invalidated the assumptions about the similarity of CD1d and pMHC proteins in relation to their interaction with TCR. In the crystal structure, the TCR was found to be positioned over the F' pocket of the CD1d-glycolipid binding cleft and not sitting perpendicularly over it as is found in the canonical pMHC/TCR binding footprint (Figure 1).

The analysis of the hydrogen bonding network between the sugar and the two proteins yielded many interesting results. The orientation of α-GalCer in CD1d in the ternary crystal structure has not changed with the addition of TCR, and its hydrogen bonding network resembles those found in the other binary CD1d/glycolipid structures. The galactose ring extends above the surface of the CD1d lipid binding groove interacting with both CD1d and TCR. Three hydrogen bonds can be identified between CD1d and α-GalCer: the 2'-OH of the galactose ring, which is crucial for the antigenicity, is hydrogen-bonded with Asp151; the 3-OH on the phytosphingosine forms a hydrogen bond with Asp80; and the glycosidic linkage 1'-O forms the third hydrogen bond with Thr154. Only Ser30 α of TCR was identified in the crystal structure as forming hydrogen bonds with the 3'- and 4'-OH groups on a galactose ring with other hydrogen bonding interactions occurring with the backbone of TCR, specifically with that of Gly96 α and Phe29 α .

Only by analyzing the interactions at the atomic level of α-GalCer with its associated proteins, CD1d and TCR, in conjunction with experimental studies will a better under-

standing of glycolipid antigenicity be achieved. The present work began with analyzing the tertiary crystal structure through molecular dynamics simulations to determine its behavior in solution and what computational methodology best reproduced experimental findings. The focus was then placed on understanding the effect of sugar modifications on the CD1d/α-GalCer/TCR tertiary crystal structure by using a combination of molecular dynamic simulations using AMBER^{42,43} and docking using Autodock⁴⁴ of a variety of glycolipids where the linkage, the sugar, or the galactose at the C2', C3', and C4' positions was modified. The four questions that were investigated were whether modifications to the sugar (1) affect binding to CD1d; (2) affect binding to the CD1d/TCR complex; (3) affect the presentation by CD1d; and (4) affect the orientation of TCR relative to CD1d.

THEORETICAL CALCULATIONS

Molecular Dynamics Solvation Environments of Ternary Complex. The starting coordinates for the molecular dynamics (MD) simulations were taken from the crystal structure of the CD1d/α-GalCer/TCR complex corresponding to the Protein Data Bank⁴⁵ entry 2PO6.⁴² In order to ascertain whether the TCR C α or C β or the CD1d β 2 regions were important for analyzing the glycolipid interaction with both proteins, a few models were created where all or some of these regions were removed. Furthermore, the lone CD1d protein and the complex without α-GalCer were also analyzed. The AMBER⁴³ molecular dynamics simulation program allowed us to explore 4 possible solvation states for these systems: 1) a fully, explicitly solvated box using TIP3P⁴⁶ waters under periodic boundary conditions (PBC) in the NVE ensemble where moles (N), volume (V), and energy (E) are conserved; 2) an explicit shell solvation where a thin layer of water is placed around the entire system but the PBC implementation is lost; 3) a spherical cap of explicit waters is used in conjunction with a “pairwise” general Born implicit solvation,⁴⁷ and 4) only a “pairwise” generalized Born implicit solvation (Figure 2).

PBC and NVE TIP3P Water Molecular Dynamics Simulations. The full protein complex is roughly twice the size of the truncated protein complex where the TCR C α /

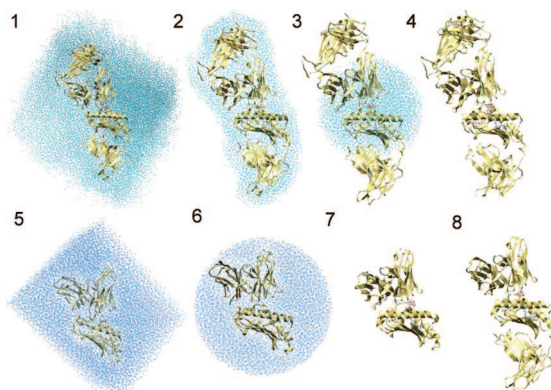


Figure 2. Different solvation environments tested in AMBER for the full and truncated complex: explicit water box solvation 1 and 5; shell and cap explicit solvation 2, 3, and 6; and implicit solvation 4, 7, and 8.

$C\beta$ and the CD1d $\beta 2$ regions were removed. The addition of hydrogens to the full protein complex yielded a system comprised of 13,063 atoms, whereas the truncated protein complex consisted of only 6497 atoms. The full complex was solvated by a $118.22 \times 57.71 \times 117.44 \text{ \AA}^3$ box totaling 40,846 TIP3P water molecules, and the truncated complex was solvated by a $89.53 \times 49.41 \times 67.45 \text{ \AA}^3$ box totaling 17,886 TIP3P water molecules. For the MD simulations, the proteins were defined by the ff03 force field,⁴⁸ whereas the α -GalCer ligand was split into sugar and lipid portions where the sugar was defined as the 1LA residue available from the Glycam⁴⁹ parameters and the lipid portion was defined using the Antechamber⁵⁰ program with the general amber force field (GAFF).⁵¹

The waters were minimized, while the complex was held frozen using an initial 500 steps of the steepest descent (SD) algorithm with an additional 500 steps to ensure complete minimization. The entire system was then minimized with an initial 1000 steps of the SD algorithm and an additional 4000 steps of minimization. With the complex fixed again, the solvent was then equilibrated to 300 K over the course of 25 ps, and then the entire system was allowed to equilibrate at 300 K for an additional 25 ps. A few additional parameters were that time steps of 2 ps were used, periodic boundary conditions were employed, the SHAKE algorithm was applied, the pressure relaxation time (taup) was set to 5.0, Langevin dynamics with a collision frequency (γ) of 1.0 was used, and a nonbonded cutoff of 16.0 \AA was employed.

Glycolipid and Docking. A library of 49 sugar modified glycolipid analogs was built using the MacroModel⁵² suite of programs. The sugars were then minimized using the PRCG method with a maximum 500 steps in water defined by the OPLS2005 force field^{53,54} with a dielectric constant of 80.0, while the lipid portion was held frozen. Snapshots taken every 1 ns of both the full and truncated explicit box solvated complex trajectories were used as receptors to which α -GalCer and the 49 glycolipids were docked. Additionally, the TCR portion was removed to determine the binding of the glycolipid to just the CD1d protein at every nanosecond.

The glycolipids were submitted to AUTODOCK⁴⁴ where the AutoDockTools package was used to generate all the necessary input files and the docking grids. The Lamarckian flexible ligand genetic algorithm search was employed. The torsions to be varied were kept under a total of 10 with the

Table 1. Molecular Dynamics Simulation Averaged Processing Data Where *Time* Is a Simulation Portion and *Real* and *CPU Time* Correspond to How Long It Took To Run That Simulation Period of Time^a

	full	truncated	implicit
atoms	13,000	6500	13,000
residues	850	400	850
waters	41,000	18,000	0
total atoms	136,000	60,500	13,000
processors	16	16	16
time	0.25 ns	0.5 ns	0.5 ns
real time	50 h	45 h	60 h
CPU time	810 h	750 h	900 h
total real (10 ns)	83 days	37 days	50 days
total CPU (10 ns)	32,400 h	15,000 h	18,000 h

^a The truncated simulation is the least expensive of the three.

minimum being 4 where every ligand had one torsion in the sphingosine and acyl chains each along with one torsion defining the glycosidic bond. The sugar substitution then yielded the rest of the torsional freedom. Each population consisted of 250 individuals, which underwent a maximum number of 5.0×10^6 energy evaluations with a maximum number of 2.7×10^4 generations and a mutation rate of 0.02 with a crossover rate of 0.8.

The free energy of binding in solvent is calculated by estimating the free energy change associated with the solvation of the protein and the ligand and then subtracting those from the free energy of binding in vacuum calculated by Autodock and from the estimated free energy change for the solvation of the complex:

$$\Delta G_{\text{binding,solution}} = \Delta G_{\text{binding,vacuo}} + \Delta G_{\text{solvation}(E)} - \Delta G_{\text{solvation}(E+1)}$$

RESULTS AND DISCUSSION

Molecular Dynamic Simulation of CD1d/ α -GalCer/TCR Complex. The elucidation of the CD1d/ α -GalCer/TCR crystal structure has given us the possibility to investigate this system on an atomic level through computational analysis. As mentioned previously, the full complex contains twice the amount of atoms as the truncated complex making it the more complex system to simulate. The first half of the simulation (~5.0 ns) was performed using the SANDER module of AMBER v8.0 on 16 Intel Itanium 2 processors with the simulation being finished using the PMEMD module of AMBER v9.0 on 16 new IBM Cluster 1350 processors. Although the simulation times were comparable, the PMEMD module was slightly faster, so Table 1 reports the molecular dynamics processing data based on the simulation times for the PMEMD module (Table 1). Simulation end points of 10.0 ns for the full complex (Figure 2.1), 16.0 ns for the truncated complex (Figure 2.5), and 10.0 ns for the implicitly solvated full complex (Figure 2.4) were performed since the 10.0 ns limit is generally accepted as the minimum necessary simulation time to determine system stability.

It was found that the best solvation environment in which to analyze the system was the full explicit water solvation under periodic boundary conditions in an NVE ensemble, which was to be expected. The PTraj module of AMBER was used to calculate the overall rmsd backbone deviations of each simulation with the exception of the shell and cap

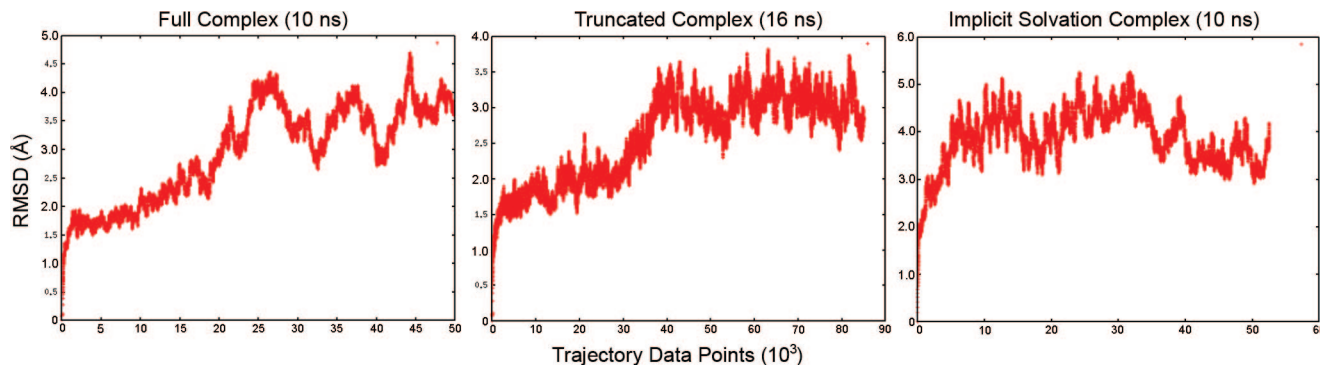


Figure 3. The rmsd simulation trajectories of the complexes show that the implicit solvation is the least stable as compared to the full and truncated complexes and that both the full and truncated follow similar rmsd deviation paths.

simulations (Figure 3). The pressure constraints of maintaining the waters within these explicit solvation environments forced the complex to not deviate at all from the crystal structure. Since the loops of TCR are assumed to be somewhat flexible, these solvation environments were believed to not provide an accurate picture of the complex's behavior in solution. The implicitly solvated truncated complexes were also disregarded due to allowing too much flexibility into the system thereby causing the complete unraveling of the proteins' structures. In the end, only simulations of the solvation environments 1, 4, and 5 were extended to the full 10.0 ns mark for complete analysis (Figure 2). The truncated complex, which was computationally less expensive, was extended to 16 ns to determine whether or not the simulation stabilized past the 10 ns point where it appeared to still be fluctuating and was found indeed to stabilize around the 3.0 Å mark. Both simulation trajectories of the full and truncated complexes showed similar trends where they gradually increased fluctuations starting at ~2.0 Å until about 5 ns at which point the system jumped to fluctuating about 3.5 Å for the full complex and 3.0 Å for the truncated. The implicit solvation trajectory did not follow the trend observed for the explicit solvation environments by rising very quickly to a rmsd of 4.0 Å. The fluctuations of the implicit system also spanned a range of ~2.0 Å in a higher frequency, whereas the explicit solvation environments had fluctuations of about ~0.5 Å; these fluctuations caused the structural disruption of the binding cavity and the erratic behavior of α -GalCer which is discussed later on.

A more extensive protein backbone rmsd analysis was performed on the individual parts comprising both protein where these portions were then found to be very relatively rigid (*see the Supporting Information* for graphs). These sections were the CD1d full protein, binding groove, and β_2 M sheet, and the TCR full protein, TCR V α , V β , C α , and C β chains (Figure 1). The binding groove fluctuated at 1.75 Å for the explicit solvation systems but around 3.0 Å for the implicit solvation where the two parallel α helices became destabilized showing that the implicit solvation could not accurately simulate them by permitting too much flexibility. The full CD1d protein is very unstable in implicit solvation fluctuating at 4.0 Å with the β_2 M sheet fluctuating very freely, whereas the explicit solvation environments show the full CD1d protein fluctuating at around 2.25, and specifically it was observed in the full complex that both the binding groove and β_2 M sheet each fluctuated at around 1.5 Å. Unlike

CD1d, the full TCR protein was shown to possess comparable stability in both the explicit and implicit solvation environments fluctuating at 2.5 Å for both. The removal of the TCR C α /C β chains to yield the truncated complex caused it to become even more rigid where the remaining TCR V α /V β chains fluctuated around 1.5 Å. Even though TCR is overall a rigid protein, the rigidity is provided specifically by the V α /V β chains, and any flexibility arises from the C α /C β chains.

The overall rmsd evaluations for the explicit solvation systems do not show the instability of the TCR and CD1d proteins but instead represent the act of TCR repositioning itself relative to CD1d as will be seen below in the analysis of the hydrogen bonding network. Furthermore, much of the flexibility in the proteins is located within the TCR C α /C β chains and the CD1d β_2 M sheet as can be seen in the truncated complex having an overall lower rmsd fluctuation compared to the full complex. Considering that the protein sections of TCR and CD1d which make up the binding pocket for the glycolipid are inherently rigid having similar rmsd fluctuations in both explicit solvent simulations and the overall trajectories up until 5 ns, it is reasonable to use the smaller and more efficient system to perform simulations on a variety of glycolipids to determine what effect they possess on the binding pocket. These results also provide support for the lock-and-key interaction proposed by Rossjohn et al. when they analyzed the binding footprint between the TCR and CD1d noticing that the proteins deviated minimally upon binding from their lone crystal structures.⁴²

A visual analysis of the fluctuations was performed by taking snapshots of the complexes every nanosecond up till 10 ns and aligning them to the 50 ps orientation (equilibrated crystal structure) using the Swiss-PDB viewer⁵⁵ (*see the Supporting Information*). The explicitly solvated complexes were found to maintain their structural integrity with only a slight shift of TCR over the F' pocket. On the other hand, the implicit solvation environment allowed too much flexibility in the system as was evident in the rmsd calculations. The flexibility was localized to CD1d causing the binding cavity to lose structural integrity thereby causing it to eject the glycolipid out of the pocket (Figure 4).

Upon observing the relative rmsd for each α -GalCer glycolipid, it can be seen that its overall binding orientation is maintained throughout the simulation with the exception for the implicit solvation system where it experienced high degrees of flexibility (Figure 5). The glycolipid at each nanosecond was removed from the complex and manually

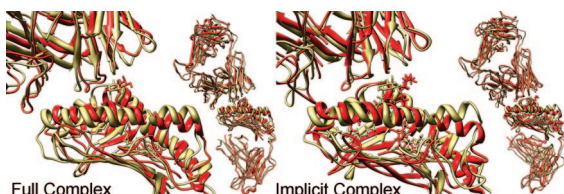


Figure 4. A view of the binding pockets for the stable explicitly solvated full complex (LH) and the extremely unstable implicitly solvated full complex (RH) where the khaki color represents 50 ps (start point) and the red color 10 ns (end point).

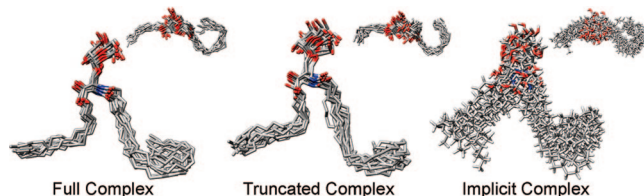


Figure 5. The manual alignment of the α -GalCer glycolipid at each nanosecond to the crystal structure orientation showed that its structural integrity and overall shape is maintained throughout the simulation with the exception of the implicit solvation where its shape becomes extremely distorted.

aligned by visual inspection for each system. It is remarkable how little the lipid portion fluctuates throughout the simulation, showing the compact space the CD1d groove forms around it. However, there is some flexibility with the sugar portion, but even this is limited due to the extensive hydrogen bonds holding it in position. The α -GalCer in the implicit solvation was observed to be ejecting itself from the binding pocket by shifting up and out of the pocket through having its lipid portions come together developing a U-shape versus the bound wavelike shape.

A few nanosecond long simulations on the truncated CD1d without α -GalCer and the truncated complex also without a ligand were performed to determine the stability of the binding pocket without a ligand. Interestingly, the simulation after 2 ns has provided us with a view of what the closed conformation of CD1d binding pocket would look like (Figure 6). Unlike in the open conformation (PDB 1ZT4) crystallized by Koch et al.³⁷ which appears to be the bound conformation of CD1d just without a ligand, the simulation showed that without a ligand the A' pocket closed up with the F' remaining open with the hinge point being the Trp153 residue. This flexibility of the A' pocket appears to show that the ligand will be loaded into the CD1d binding groove by entering the F' pocket causing the A' pocket to slowly open and accommodate the ligand. Furthermore, this also shows the importance of having the appropriate length acyl chain or spacer molecule as was done with GalA-GSL³⁸ so as to provide the correct shape for CD1d to interact most effectively with TCR; so even though the A' pocket forms no contacts with TCR, the rotation of the helices inward at this end cause the F' pocket residues to be displaced enough to not be in an optimum orientation to form the necessary contacts with TCR.

An Analysis of the Hydrogen Bond Network in the CD1d/ α -GalCer/TCR Complex. The most revealing information ascertained from the crystal structure is the binding footprint of TCR onto CD1d. The molecular dynamics simulations did not show TCR reverting to the binding footprint it has with the MHC proteins nor did they show it

disengaging itself from CD1d. This data provides some additional support that this is indeed the binding footprint between TCR and CD1d. Of course, to observe such a dramatic rotation would require much longer simulations. The prominent recognition force between these two proteins that creates this interesting binding footprint is the hydrogen bond network. Furthermore, the network formed between the glycolipid and both proteins drives glycolipid binding, recognition, and discrimination. Therefore, the permanence of these important hydrogen bonds throughout the simulation was closely investigated. The results were compared to the network found in crystal structure⁴² along with mutation studies⁵⁶ performed on these key residues.

The ptraj module was used once again to analyze the full and truncated complex simulations to determine the permanence of the hydrogen bonds as was a visual inspection performed at varying time intervals (Table 2, Figure 7). The network between the α 1 helix of CD1d and the TCRV α /V β chains provides for the unusual binding footprint of this complex. Although the TCR protein sits atop the whole F' pocket of CD1d, there are no hydrogen bonds between the α 2 helix of CD1d and TCR. Based on the crystal structure, there are two hydrogen bond webs between the α 1 helix of CD1d and TCR. The web existing by the far end of the F' pocket has as its focus the Glu83 residue to which then Lys86, Tyr48 β , and Tyr50 β are bonded. The second hydrogen bond web occurs in the middle of the α 1 helix with Arg79 being its focus where Arg103 α , Asp94 α , and Arg95 α were hydrogen bonded to it, and through Arg95 α the web also included Asp80 and Ser76 located on the α 1 helix.

The simulations showed that these hydrogen bond webs were in flux; however, the Glu83 and Arg79 residues still remained the focus of each hydrogen bond web. The Glu83 forms the most permanent hydrogen bond with Arg103 α in both complexes where this residue was not shown to be hydrogen bonded to Glu83 in the crystal structure. The flexibility of the arginine residue allowed for it to swing over quite early on in the simulation. In the full complex, the hydrogen bond web involving Tyr48 β , Tyr50 β , and Lys86 for the Glu83 was maintained for ~50% of the simulation; however, this web is less prevalent in the truncated complex where it existed <10% of the time. As the simulation progressed, this hydrogen bond web began strong and then faded away, just more quickly for the truncated complex. With the loss of these hydrogen bonds a slight shift of the TCR complex off the F' pocket was observed. The shift was also likely due to the Arg103 α swinging over to form hydrogen bonds to Glu83 thereby bringing the TCR with it. Correlating these results to the mutation studies carried out, it was found that the Glu83Ala mutation had a massive impact on the binding affinity as could be expected since it is the focal point of one of the hydrogen bond webs and without it all would be lost. Interestingly, the Arg103 α Ala mutation had no effect on binding affinity implying that its nonexistence can be supplanted by the other residues of the web. The Tyr48 β Ala and Tyr50 β Ala mutations were also critical to the binding affinity. This was unusual because it would be expected that one tyrosine could compensate for the loss of the others hydrogen bond capabilities as could the Arg103 α . Considering that in the simulation the hydrogen bonds between the tyrosines and Glu83 were not well maintained, it is quite possible that their importance lies in

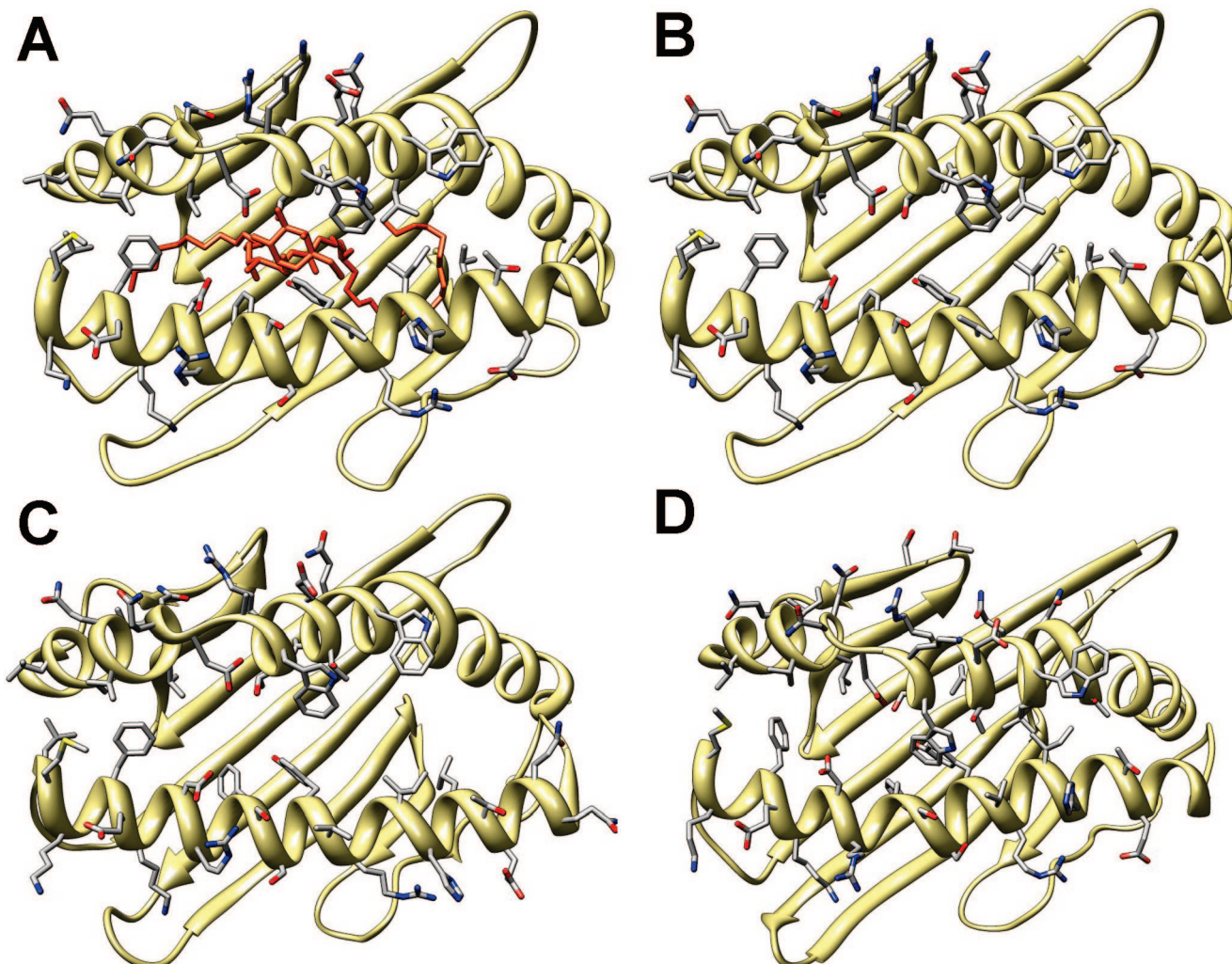


Figure 6. Unbound and bound states of CD1d binding groove: (A) tertiary crystal structure CD1d binding groove with α -GalCer bound; (B) tertiary crystal structure CD1d binding groove with α -GalCer removed; (C) crystal structure of open conformation; and (D) closed conformation of CD1d binding groove after 2 ns of simulation.

providing other electrostatic stabilizing interactions with the $\alpha 1$ helix that outweigh the hydrogen bonding interactions.

The other focal point residue, Arg79, of the hydrogen bond web close in the middle of CD1d and close to the sugar headgroup maintained its hydrogen bond to Asp94 α for 90% of the full complex simulation but only about 30% of the time for the truncated complex, again only at the beginning. The Arg79 residue, even though it is the focus of the second hydrogen bond web, was found to not be as important a $\alpha 1$ helix residue as the Glu83 where its Arg79Ala mutation had no adverse effect on binding. On the other hand, the Asp94 α Ala and Arg95 α Ala mutations did drastically affect the binding affinity of TCR to CD1d. Since Asp94 α hydrogen bonds to Arg79, an unimportant residue, it can be assumed that the Asp94 α Ala mutation causes a displacement of the Arg95 α making it then the important residue in this web being hydrogen bonded to Asp80. In the case of the full complex, the hydrogen bond between Asp80 and Arg95 α is prevalent for 85% in the full complex and 50% in the truncated complex. This is also the most permanent hydrogen bond between CD1d and TCR for the truncated complex and the second most in the full complex. The Asp80 residue not only maintained a hydrogen bond with TCR but also exhibited the most permanent hydrogen bonding in both

complexes with the hydroxyl groups of the sphingosine chain, existing >90% of the time with both. Therefore, Asp80 located on CD1d is the most important residue in the system by forming strong and lasting hydrogen bonds with both TCR and α -GalCer.

The last hydrogen bond web has the galactose sugar of the α -GalCer glycolipid as its focus. During the simulation, the Asp151 which is thought to be strongly bonded to the 2'-OH of the galactose whose removal, 2'-deoxy, causes the glycolipid to lose all activity prefers instead to hydrogen bond to the 3'-OH by a difference of >50% permanence between the two hydrogen bonds. This preference is furthered by Asp151 hydrogen bonding to the backbone of Thr154 85% of the time, thereby drawing the Asp151 away from the 2'-OH and closer to the 3'-OH. The Ser30 α residue appeared to form a hydrogen bond with the galactose sugar of α -GalCer in the crystal structure; however, its Ser30 α Ala mutation did not affect the binding affinity of TCR to CD1d, and it only remains hydrogen bonded to the 2' and 3'-OHs for <10% of the time. Overall, the galactose sugar remains within its binding pocket between TCR and CD1d maintaining its overall orientation and hydrogen bonds.

The Swiss-PDB Viewer was used to align the crystal structure, the full complex, and truncated complex at 3 ns,

Table 2. Permanence of the Hydrogen Bonds between Key Residues' Atoms Throughout the 10 ns Simulation Where %Oc Refers to the Period of Time of the Simulation That Hydrogen Bond Was Occupied, i.e. Maintained^a

full complex			truncated complex		
donor	acceptor	%Oc	donor	acceptor	%Oc
Asp80	AGH_O4	96.79	Asp80	AGH_O4	97.84
Asp80	AGH_O3	92.27	Asp80	AGH_O3	93.63
Asp94 α	Arg79	90.70	Asp151	ILA_O3	93.27
Asp151	Thr154	85.46	Asp151	Thr154	83.53
Asp80	Arg95 α	84.35	Asp80	Arg95 α	49.78
Asp94 α	Arg79	83.50	Glu83	Arg103 α	37.35
Asp151	ILA_O3	82.78	Asp80	Arg95 α	35.43
Glu83	Arg103 α	60.02	Asp94 α	Arg79	33.27
Glu83	Tyr50 β	57.09	Asp94 α	Arg79	30.35
Glu83	Tyr48 β	54.79	Glu83	Arg103 α	20.38
Glu83	Arg103 α	30.07	Glu83	Arg103 α	19.90
Glu83	Lys86	29.63	AGH_O	ILA_O2	19.51
Asp151	ILA_O2	24.25	Asp94 α	Arg79	19.06
Asp94 α	Arg79	20.19	AGH_O	Thr154	13.72
Glu83	Lys86	15.98	ILA_O3	Ser30 α	11.90
Glu83	Lys86	13.94	Glu83	Tyr48 β	10.46
Asp151	ILA_O3	13.53	ILA_O4	Ser30 α	10.07
Asp151	Thr154	12.66	Asp151	ILA_O2	10.05
Glu83	Tyr50 β	12.02	Glu83	Tyr50 β	9.16
Glu83	Arg103	8.39	Asp94 α	Arg79	9.13
ILA_O3	Ser30 α	6.79	Glu83	Lys86	8.10
AGH_O1	ILA_O2	6.70	Glu83	Arg103 α	7.08
ILA_O4	Ser30 α	5.87	Glu83	Lys86	5.80

^a Specific atoms are not shown for the residues below, but see the Supporting Information for these and additional statistics. AGH refers to the lipid portion of α -GalCer, and ILA refers to its galactose headgroup. ILA_O# refers to hydroxyls on the galactose sugar, AGH_O1 is the glycosidic bond linking the lipid and sugar portions, AGH_O is the amide carbonyl on the acyl chain, and AGH_O# are the hydroxyls on the sphingosine chain.

before the rmsd shift to a higher deviation, and at the 10 ns mark, in order to provide a visual idea of how CD1d/ α -GalCer/TCR interact during the simulation (Figure 7). It is important to point out that the rmsd of the trajectories appear to make the situation more drastic than it truly is when comparing the crystal structure to the 3 and 10 ns final orientations. Interestingly, an arginine stack forms by 3 ns and is maintained more or less throughout the simulation involving the Arg95 α , Arg79, and Arg103 α residues. This arginine stacking quite possibly plays a prominent role in disrupting the tyrosine hydrogen bonds with Glu83 thereby causing the shift of the CDR2 β . However, the tyrosines' hydrogen bond network still exists at 3 ns, and it is not disrupted until the 10 ns mark in both complexes. Three other residues that do not participate in hydrogen bonding but do provide van der Waals interactions with the sugar are also important to discuss. The Phe51 α and Trp153 in the crystal structure are separated by 6.7 Å which appears to be a large enough distance for the Phe51 α to adopt an edge to face orientation rather than an offset or stacked orientation relative to the Trp153 creating a barrier behind the 4'-OH position. This closing creates a more compact electrostatic pocket for the galactose; however, it probably adds to the overall shifting of the TCR off the F' pocket in hinge fashion. The Arg95 α also behaves in a similar fashion by angling in more toward the C1' position thereby further compacting the space within which the sugar sits. This propensity for the TCR cavity surrounding the sugar to compact even more so around

the sugar provides support for why modifications to it are not very tolerated by the system.

In summary, it appears that the hydrogen bonding interactions between the CD1d/ α -GalCer/TCR evolve as the simulations progress. The loss of hydrogen bonds and the formation of new ones was correlated to the shifting of TCR slightly over the F' pocket of CD1d. This repositioning cannot be considered an instability and hence unreliability in the simulations but should be an expected motion for these two proteins. To begin with, the total buried surface area between TCR and CD1d is quite small at ~910 Å² compared to the buried surface area between TCR and MHC proteins, implying that there are less stabilizing interactions between TCR and CD1d and therefore more ability to move relative to each other. Furthermore, TCR and CD1d remain relatively rigid around the binding footprint exhibiting a lock-and-key type interaction, where this type of protein binding interactions requires TCR and CD1d to come together in roughly the correct orientation, so a slight shift of TCR relative to CD1d implies a larger keyhole. The crystal structure is one stable, frozen representation of this system that was able to be crystallized. The structures resulting from simulation are additional representations for how this system behaves in solution.

Glycolipid Autodock Results. A library of 49 glycolipid analogs was built where the sugar was replaced or various substitutions were made at the C2', C3', or C4' positions to investigate the role of the sugar in the CD1d/glycolipid/TCR binding event (Chart 1). It is well-known that substitutions at the C2' positions are not tolerated resulting in TCR not binding CD1d, whereas substitutions at the C6' position of the sugar are extremely well tolerated with even large groups or additional sugars able to be placed on there.⁵⁷ However, only recently have the C3' and C4' positions come under investigation where 3'- and 4'- deoxy analogs of α -GalCer were found to bind TCR and stimulate a response.⁵⁶ It was hypothesized by the authors that the C3' substitutions would be less tolerated than the C4' positions which experimental evidence from our laboratory has been able to support (*unpublished results*).

The AUTODOCK v3 program was utilized to determine the binding energies of the glycolipid analogs. The first group of analogs (PGW001-006) was built to correlate their binding energies to currently available experimental evidence where it has been shown that CD1d can bind both α and β linked sugars; however, β linked sugars cannot be recognized by TCR,⁵⁸ that the 4'-OH can be either equatorial or axial (Gal versus Glc)⁵⁹ and that a carboxylic acid group at the 6' position (GSL) also causes a TCR response.⁶⁰ The second group of analogs (PGW20X, PGW30X, and PGW40X) were created to analyze whether or not a preference could be found between the C2', C3', or C4' positions when analyzing binding energies. The substitutions involved deoxy to eliminate the hydrogen bond capabilities of the position, methoxy to eliminate the hydrogen bond donor capabilities, a group of amine derivatives, and two bulkier substituents. Based on previous lines of evidence and the crystal structure of the tertiary complex, a library of C4' analogs (PGW50X and PGW6XX) was built to analyze how bulky of a substitution would be tolerated at the position, whether the Phe51 α and Trp153 could lend themselves to π - π interactions with the substituent, and if the flexibility of the

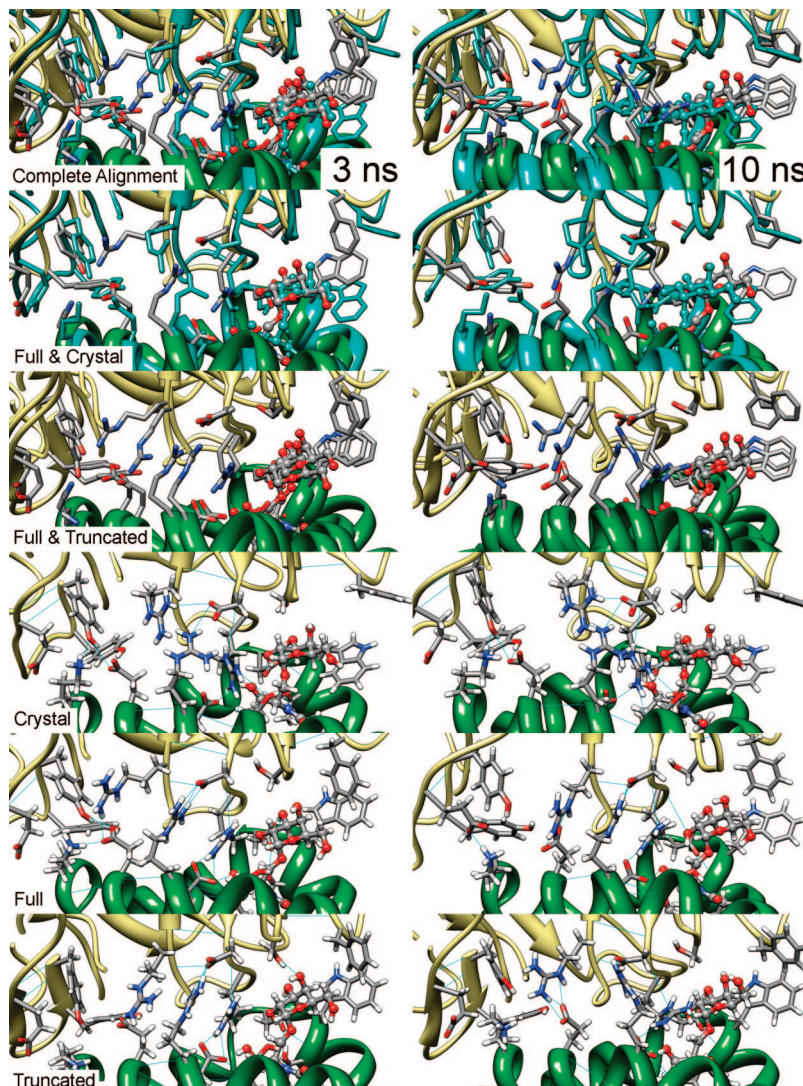


Figure 7. The alignment of the crystal structure, the full complex, and truncated complex at the 3 (LH) and 10 ns (RH) marks in order to provide a visual idea of how CD1d/ α -GalCer/TCR interaction evolves during the simulation. In the complete alignment and full and crystal images the crystal structure is colored cyan, and in each picture TCR is khaki and CD1d is green. The hydrogens were removed from the overlapping structures to provide a clearer image, whereas in the individual proteins' images they were maintained to show the hydrogen bonding network. Residue labels were also omitted for the sake of clarity.

substituent as determined by the sugar linkage (ester, ether, or amide) played a role in binding.

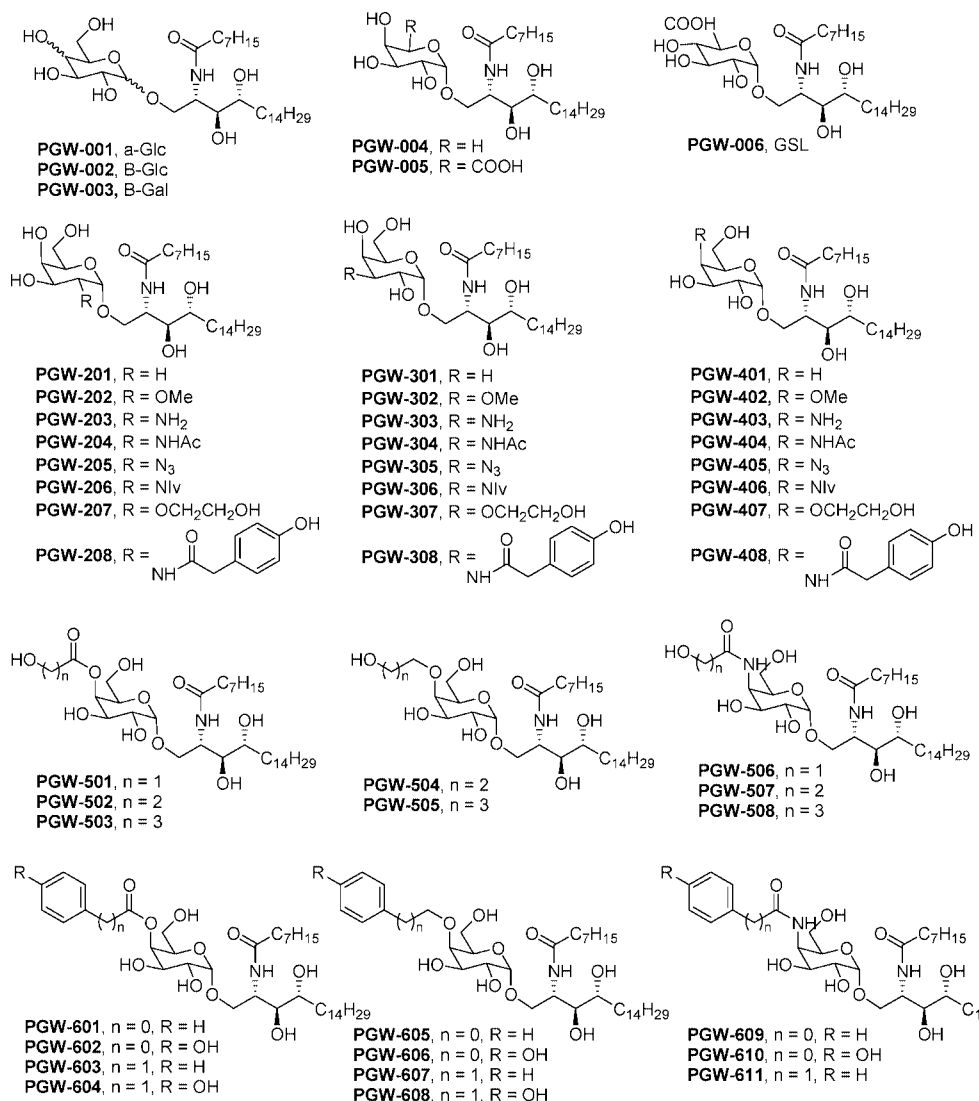
The most unusual result of the binding experiments was that α -GalCer was neither the best nor the worst ligand, implying that it may be quite possible that binding energies are not solely responsible for determining whether a specific glycolipid is a good ligand to stimulate iNKT cells. Three sets of binding energies were obtained from the simulations: binding to the crystal structure, overall tertiary complex binding, and binding to the CD1d protein. A hypothetical TCR binding energy was calculated by assuming that the glycolipid to tertiary complex binding energy is made up of the binding to CD1d and to TCR; therefore, subtracting the complex binding energy from the CD1d binding energy would yield the binding energy to TCR of the glycolipid. This is a different value than the binding of the CD1d/ α -GalCer binary complex to TCR; it instead shows the favorability of the glycolipid interaction with TCR. Currently, protein–protein docking would be the only recourse to calculate the CD1d/ α -GalCer binary complex to TCR binding energy; however, this is still a very underdeveloped area of

docking and AUTODOCK is not built for it. The values shown here are the average binding energies determined along with the worst (MAX) binding energy from all of the docked trials (Table 3, *for an extensive listing see the Supporting Information*). The average energies for all four sets of data show a range of ~ 3 kcal/mol from the best to worst binding analog, whereas the MAX energies span a range of 5–8 kcal/mol between the best and worst analogs.

Teyton et al.⁶¹ have determined dissociation constants (K_D) for α -GalCer to mouse CD1 (mCD1) to be 2.3 and 5.9 μM using IEF and 1.0 and 9.7 μM using ITC. These K_D values were converted to free energy values following the Autodock methodology⁴⁴

$$\Delta G_{obs} = RT \ln K_D$$

where R is the gas constant, 1.987 cal $\text{K}^{-1} \text{mol}^{-1}$, and T is the absolute temperature, 298.15 K, yielding values of -7.691 , -7.133 , -8.185 , and -6.839 kcal/mol which averaged out to -7.462 kcal/mol. Considering that both mCD1 and human CD1d are similar and can both present α -GalCer to iNKT cells, it is reasonable to extrapolate that

Chart 1. List of 49 Various Sugar Modified Glycolipids Built and Docked into the CD1d/TCR Tertiary Complex and the CD1d Protein

they will have similar binding energies for α -GalCer. The average binding energy from docking for α -GalCer was found to be -7.43 kcal/mol which is nearly identical to the experimentally determined value.

Upon comparing the CD1d binding energies between all the glycolipids, it appears that they should all bind CD1d with similar efficacy, which has been found to be the case considering that current experimental studies require the glycolipids to be loaded onto CD1d and presented to TCR. If the binding energy of α -GalCer was either the lowest or the highest, it would be easy to conclude that glycolipids with binding energies close to α -GalCer should behave similarly; however, this is not the case with α -GalCer possessing lower average binding energies than most of the glycolipids. Nevertheless, maintaining the same argument, the cluster of glycolipids surrounding α -GalCer was considered. Based on experimental evidence from our laboratory, C3' α -GalCer analogs were found not to elicit an iNKT cell response, whereas C4' substituted analogs did. Assuming that the binding energy can indeed be correlated to iNKT cell response, it can be seen that the average energies of the C2', C3', or C4' substituted analogs do not follow this iNKT response trend with them being dispersed among each other especially around α -GalCer. However, the MAX binding

energies appear to support the hypothesis that there should be a difference in binding between the C2', C3', or C4' substituted α -GalCer analogs when analyzing their potential in iNKT cell stimulation.

The α -Glc, β -Glc, and β -Gal were found to bind CD1d better than α -GalCer, whereas the C6' modified sugars had worse binding energies than α -GalCer. Experimentally, β linked sugars yield no TCR response which correlates to their worse TCR binding energies as compared to α -GalCer, whereas GSL and its derivative along with α -Glc are supposed to elicit a TCR response which correlates to their improved TCR binding energies. The 6'-deoxy analog, due to the hydrophobic nature of the C6' position, yields unfavorable binding. Overall, all these monosaccharide analogs bind to the complex with improved affinity as compared to α -GalCer.

When comparing the C2', C3', or C4' substituted analogs using α -GalCer as the dividing point, it appears that the C4' analogs are overall better binders to the complex, with a few that are poor CD1d binders and only a few that bind well to TCR, as compared to the C2' and C3' substituted sugars which exhibited an overall poor complex, CD1d, and TCR binding, especially as the bulkiness of the group increased.

Table 3. Binding Energies in kcal/mol for the Tertiary Complex, the CD1d Protein, and the TCR Protein^a

crystal structure	average energies (kcal/mol)						MAX energies (kcal/mol)						
	complex		CD1d		TCR		complex		CD1d		TCR		
PGW508	-14.86	PGW503	-12.38	PGW303	-8.66	PGW503	-3.97	PGW507	-7.59	PGW003	-4.99	PGW505	-2.50
PGW507	-14.76	PGW505	-12.30	PGW608	-8.54	PGW504	-3.84	PGW504	-7.44	PGW002	-4.89	PGW407	-2.09
PGW505	-14.65	PGW502	-11.93	PGW505	-8.46	PGW502	-3.79	PGW606	-6.92	PGW603	-3.99	PGW601	-2.01
PGW504	-14.62	PGW504	-11.76	PGW503	-8.35	PGW505	-3.79	PGW501	-6.81	PGW205	-3.81	PGW304	-1.92
PGW502	-14.42	PGW508	-11.41	PGW508	-8.32	PGW407	-3.67	PGW502	-6.73	PGW206	-3.77	PGW605	-1.83
PGW503	-14.40	PGW501	-11.31	PGW301	-8.29	PGW501	-3.62	PGW503	-6.68	PGW608	-3.74	PGW006	-1.68
PGW208	-14.21	PGW303	-11.30	PGW604	-8.25	PGW304	-3.51	PGW604	-6.56	PGW503	-3.69	PGW402	-1.68
PGW207	-14.04	PGW606	-11.27	PGW404	-8.22	PGW307	-3.47	PGW505	-6.48	PGW607	-3.68	PGW005	-1.63
PGW408	-13.61	PGW608	-11.25	PGW502	-8.10	PGW308	-3.46	PGW506	-6.43	PGW504	-3.65	PGW405	-1.60
PGW407	-13.61	PGW507	-11.19	PGW507	-8.08	PGW207	-3.42	PGW408	-6.28	PGW505	-3.57	PGW001	-1.45
PGW205	-13.61	PGW205	-11.19	PGW203	-8.03	PGW606	-3.34	PGW508	-6.22	PGW604	-3.57	PGW501	-1.29
PGW307	-13.57	PGW604	-11.18	PGW003	-8.01	PGW005	-3.31	PGW407	-6.18	PGW601	-3.52	α -GalCer	-1.22
PGW506	-13.41	PGW407	-11.17	PGW603	-7.98	PGW405	-3.29	PGW601	-6.09	PGW402	-3.50	PGW305	-1.22
PGW303	-13.32	PGW602	-11.12	PGW610	-7.97	PGW205	-3.25	PGW608	-6.09	PGW408	-3.50	PGW201	-1.11
PGW308	-13.32	PGW307	-11.11	PGW504	-7.94	PGW601	-3.18	PGW005	-5.95	PGW502	-3.48	PGW604	-1.09
PGW501	-13.29	PGW405	-11.08	PGW606	-7.94	PGW605	-3.15	PGW605	-5.86	PGW203	-3.47	PGW004	-1.06
PGW405	-13.26	PGW003	-10.95	PGW205	-7.89	PGW006	-3.13	PGW006	-5.80	PGW001	-3.42	PGW205	-1.01
PGW604	-13.25	PGW308	-10.82	PGW208	-7.89	PGW507	-3.11	PGW602	-5.71	PGW403	-3.39	PGW207	-0.95
PGW608	-13.12	PGW304	-10.82	PGW607	-7.88	PGW506	-3.04	PGW404	-5.67	PGW507	-3.39	PGW401	-0.82
PGW611	-13.08	PGW002	-10.80	PGW408	-7.88	PGW002	-3.03	PGW402	-5.65	PGW404	-3.34	PGW408	-0.72
PGW304	-13.07	PGW601	-10.79	PGW406	-7.80	PGW402	-3.02	PGW002	-5.56	α -GalCer	-3.31	PGW502	-0.72
PGW404	-12.99	PGW207	-10.78	PGW206	-7.80	PGW508	-3.00	PGW301	-5.56	PGW609	-3.29	PGW002	-0.67
PGW306	-12.98	PGW605	-10.74	PGW002	-7.79	PGW602	-2.93	PGW003	-5.54	PGW401	-3.27	PGW608	-0.66
PGW204	-12.89	PGW610	-10.67	PGW405	-7.75	PGW003	-2.93	PGW403	-5.44	PGW610	-3.22	PGW003	-0.55
PGW606	-12.88	PGW203	-10.65	PGW601	-7.74	PGW604	-2.92	PGW401	-5.22	PGW301	-3.14	PGW302	-0.54
PGW610	-12.82	PGW208	-10.65	PGW201	-7.71	PGW201	-2.89	PGW001	-4.98	PGW611	-3.09	PGW603	-0.52
PGW202	-12.80	PGW301	-10.63	PGW501	-7.69	α -GalCer	-2.87	PGW609	-4.92	PGW508	-3.00	PGW307	-0.36
PGW602	-12.71	PGW404	-10.60	PGW602	-7.68	PGW305	-2.84	α -GalCer	-4.90	PGW201	-2.87	PGW301	-0.27
PGW305	-12.68	PGW408	-10.60	PGW605	-7.60	PGW302	-2.83	PGW305	-4.88	PGW305	-2.84	PGW303	-0.25
PGW607	-12.63	PGW006	-10.59	PGW402	-7.59	PGW001	-2.83	PGW205	-4.82	PGW006	-2.72	PGW506	-0.16
PGW006	-12.59	PGW201	-10.59	PGW609	-7.58	PGW408	-2.69	PGW610	-4.81	PGW302	-2.65	PGW607	-0.16
PGW601	-12.54	PGW402	-10.53	PGW305	-7.57	PGW610	-2.69	PGW307	-4.65	PGW307	-2.65	PGW504	-0.05
PGW605	-12.45	PGW603	-10.47	PGW307	-7.57	PGW608	-2.69	PGW308	-4.62	PGW407	-2.56	PGW403	-0.04
PGW005	-12.42	PGW005	-10.46	PGW407	-7.50	PGW004	-2.65	PGW603	-4.51	PGW202	-2.52	PGW610	0.03
PGW609	-12.41	PGW607	-10.44	PGW403	-7.50	PGW208	-2.63	PGW405	-4.38	PGW005	-2.51	PGW503	0.04
PGW603	-12.37	PGW506	-10.43	PGW004	-7.48	PGW401	-2.62	PGW203	-4.30	PGW207	-2.44	PGW203	0.05
PGW206	-12.36	PGW305	-10.35	PGW006	-7.44	PGW203	-2.61	PGW304	-4.22	PGW501	-2.44	PGW308	0.31
PGW402	-12.31	α -GalCer	-10.30	α -GalCer	-7.43	PGW607	-2.56	PGW201	-3.98	PGW204	-2.42	PGW606	0.33
PGW403	-12.27	PGW001	-10.25	PGW204	-7.41	PGW303	-2.55	PGW607	-3.84	PGW405	-2.42	PGW208	0.36
PGW203	-12.13	PGW004	-10.14	PGW506	-7.41	PGW202	-2.53	PGW207	-3.65	PGW303	-2.35	PGW204	0.43
PGW302	-12.12	PGW403	-10.02	PGW611	-7.41	PGW603	-2.49	PGW004	-3.19	PGW004	-2.13	PGW609	0.43
PGW201	-12.10	PGW609	-9.99	PGW202	-7.39	PGW403	-2.49	PGW202	-3.19	PGW304	-1.84	PGW507	0.81
PGW004	-12.05	PGW202	-9.93	PGW207	-7.34	PGW301	-2.45	PGW302	-3.19	PGW406	-1.61	PGW202	0.89
α -GalCer	-12.05	PGW204	-9.86	PGW308	-7.32	PGW609	-2.41	PGW303	-2.85	PGW208	-1.42	PGW508	1.12
PGW001	-12.01	PGW302	-9.83	PGW304	-7.29	PGW204	-2.39	PGW208	-2.39	PGW308	-1.31	PGW404	2.64
PGW301	-12.00	PGW401	-9.69	PGW401	-7.19	PGW404	-2.34	PGW204	-1.99	PGW606	-1.19	PGW306	2.91
PGW003	-11.91	PGW206	-9.66	PGW001	-7.16	PGW306	-2.25	PGW306	-1.18	PGW506	-1.15	PGW206	4.92
PGW406	-11.90	PGW611	-9.53	PGW005	-7.14	PGW206	-1.93	PGW206	-0.05	PGW306	-0.12	PGW602	5.48
PGW401	-11.77	PGW306	-9.34	PGW306	-7.09	PGW611	-1.55	PGW611	0.05	PGW602	0.12	PGW611	8.16
PGW002	-11.43	PGW406	-9.32	PGW302	-7.09	PGW406	-1.50	PGW406	1.12	PGW605	0.62	PGW406	8.29

^a Average energies represent the average from all docked trials, and MAX energy represents the worst binding energy out of all the docked trials.

Experimentally, it was found that PGW402 and PGW407 do elicit a comparable TCR response to that of α -GalCer correlating to their improved TCR binding (*unpublished results*). Lastly, it appears that the alkyl hydroxyl PGW50X compounds overall are better binders to the tertiary complex owing to their flexibility; however, only a few contribute specifically to TCR binding. When it comes to the bulkiness of the substituents, the overall trend appears that the bulkier the substituent (phenols and NIv) with the less flexible linker (an amide) the lower the binding energy. Considering that the binding energy values differ sometimes \sim 0.02 kcal/mol between compounds, it is the trends that must be observed and with less focus being placed on the actual energy values.

On the other hand, these differences are similar to the minimal differences between the binding energies of TCR to the CD1d/glycolipid binary complexes tested by Kronenberg et al.⁶² where the values ranged from -6 to -8 kcal/mol.

Molecular Dynamic Simulations on a Choice CD1d/Glycolipid/TCR Truncated Complexes. A few chosen docked CD1d/glycolipid/TCR tertiary complexes were submitted to molecular dynamics simulations where the proteins, which were held rigid in the docking runs, were allowed to relax and equilibrate to the presence of the new glycolipid. It was hypothesized that in the MD simulation the sugar modifications will cause the orientation of the glycolipid,

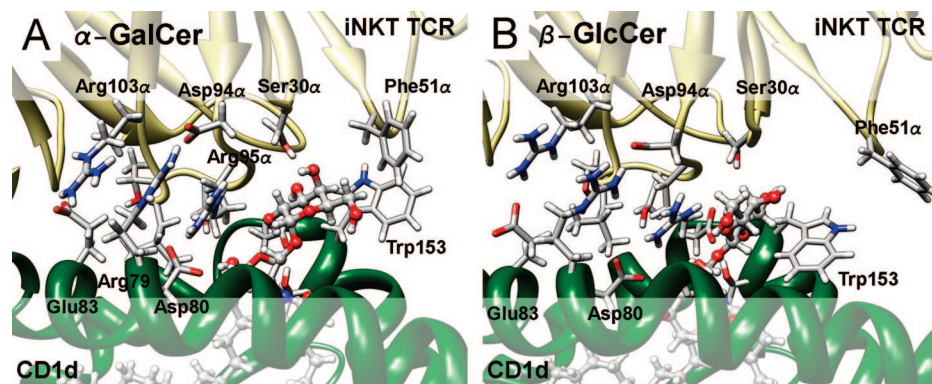


Figure 8. The orientations of (A) α -galactose and (B) β -glucose sugars after 3 ns of simulation.

TCR, CD1d, or the entire complex to change; therefore, the following analogs were chosen to perform 3 ns simulations on: β -GlcCer (PGW002) to determine the effect of the glycosidic linkage on the orientation of the complex: 2'-, 3'-, and 4'-NHAc- α -GalCer (PGW402-404); 2'-, 3'-, and 4'-OMe- α -GalCer (PGW302-304); and 2'-, 3'-, and 4'-HE- α -GalCer (PGW307, PGW308, PGW505) to determine the effect of substitutions on the galactose sugar; and PGW306, PGW508, and PGW408 to determine the effect of bulky aromatic substituents at the C2' and C4'-position.

The truncated CD1d/glycolipid/TCR complex in explicit solvent was chosen to perform less intensive and hence more simulations. The 3 ns mark was chosen as an end point to the simulations because both the full and truncated complexes appeared to behave similarly until this point. Furthermore, it was hypothesized that any modification of the sugar will be immediately felt by the complex, and its structural motions will be directed at accommodating this novel glycolipid. This hypothesis was supported by the rmsd calculations of the simulations where the C4' complexes showed stable trajectories that fluctuated between 2.5–3.0 Å similar to the truncated TCR/ α -GalCer/CD1d simulation, whereas the C2' and C3' analogs' trajectories were more unstable and fluctuating between 3.0–3.5 Å and appeared to be increasing versus stabilizing as did the C4' trajectories. This may point to the fact that C2' and C3' analogs deny a stable tertiary structure to be formed upon TCR recognition of the CD1d binary complex, whereas C4' analogs allow the creation of a stable tertiary structure.

As in the crystal structures of CD1d/sulfatide²⁸ and CD1d/iGb3³⁹ where the sugars were attached to the lipid portion by a β linkage, the simulated β -GlcCer adopted a similar perpendicular orientation projecting out of the cavity rather than the flatter orientation of α -GalCer (Figure 6). There are no differences in the hydrogen bond network between the proteins for both glycolipids, implying that β -GlcCer does not affect the recognition between TCR and CD1d. The orientation of the β -glucose does, however, cause the important hydrogen bonding to the Gly96 α to be lost, while simultaneously allowing the 6'-OH to form a new hydrogen bond with Ser76 on the α 1 helix of CD1d. Considering that β -GalCer has been found to very weakly stimulate iNKT cells⁶³ whereas β -GlcCer was found not to be able to stimulate them at all,⁶⁴ it is possible that in this case the 4'-OH in β -GalCer plays a critical role by reforming the hydrogen bond to the Gly96 α since its orientation would be toward the CDR3 α loop, whereas in β -GlcCer it is toward the CDR2 α loop.

The CDR2 α loop containing Phe51 α shifted drastically away during the simulation of β -GlcCer from the Trp153 and the C4' position, thereby opening up a space between it and the CDR1 α loop that measures roughly ~8 Å in width from Ser30 α to Phe51 α (Figure 8B). Many currently tested diglycosylceramides are derivatives of the α -GalCer and not β -GlcCer,⁶⁵ and since there is no space for the second sugar at either the C2', C3', or C4' position (Figure 8A), these are only tolerated upon being truncated by a glycosidase back to the α -GalCer. However, the opening at the C4' position of β -GlcCer provides evidence for why iGb3 has been found to be a viable glycolipid. At the same time, the disaccharide Gal β 1-4Glc β 1-1'Cer was found to be incapable of stimulating V α 14 NKT cells²⁹ showing that the disaccharide even though it could fit into this opening probably does not form necessary electrostatic interactions to ensure TCR stimulation, which is why the third sugar is needed.

The 3 ns MD simulations of the C2'-, C3'-, and C4'-analog's tertiary complexes showed that many events occurring simultaneously more than likely contribute to the lack of iNKT cell stimulation for the C2'- and C3'-glycolipids (Figure 9). The most obvious difference between the substitutions is the orientation of the sugar and its hindered ability to form the necessary hydrogen bonds within its binding pocket. Only the C4' analogs maintain all the necessary hydrogen bonds that exist between the 2'- and 3'-OHs and TCR, thereby allowing it to maintain a similar orientation as α -GalCer inside the binding pocket (Figure 9C,F,I,K,L). This is in contrast to the 2'-, 3'-OME and HE analogs where the sugar rotates slightly for the 3'-OH to compensate for the lack of hydrogen bond donating of the C2' substituent to Asp151 and vice versa. In the 2'- and 3'-NHAc analogs, the sugar orientation is more drastically affected, where the 2'-NHAc analog adopts an orientation reminiscent of β glycolipids and the 3'-NHAc analog forms none of the necessary hydrogen bonds to Gly96 α , Asp151, nor Thr154 due to the fact that the sugar is being ejected from the binding pocket, whereas the 4'-NHAc, like the other C4'-analogs, maintains similar orientation and hydrogen bonding as α -GalCer. However, the loss of hydrogen bonding due to incorrect sugar orientation cannot be the sole determining factor for iNKT cell stimulation otherwise such logic as improving hydrogen bond donating/accepting groups on the C2'- and C3'-positions would not have failed.

A more important consequence of these analogs is that half of the hydrogen bonding network between CD1d and TCR is disrupted. The hydrogen bond network between Glu83, Lys86, Tyr48 β , and Tyr50 β is disrupted by Arg103 α

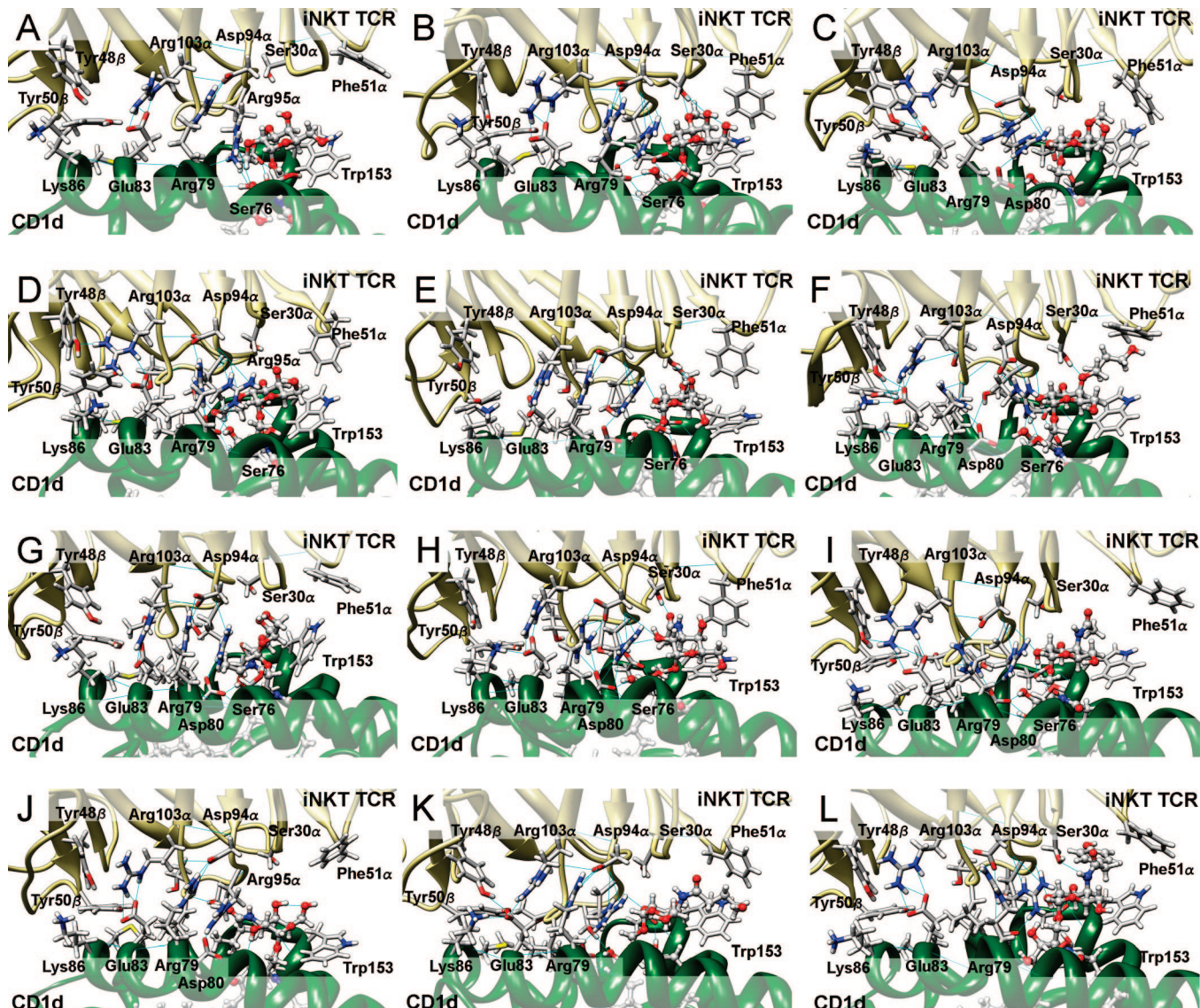


Figure 9. The CD1d/glycolipid/TCR truncated tertiary complexes after undergoing 3 ns MD simulations: (A-C) 2', 3'-, and 4'-OMe- α -GalCer; (D-F) 2', 3'-, and 4'-HE- α -GalCer; (G-I) 2', 3'-, and 4'-NHAc- α -GalCer; and (J-L) 2'-NIV- α -GalCer PGW306, C4'- α -GalCer PGW508, and C4'- α -GalCer PGW408, respectively.

swinging over and forming hydrogen bonds with Glu83 for the C2'- and C3'-analogs, thereby not allowing the tyrosines and lysine residues to form hydrogen bonds, but this is not the case for the C4'-analogs, whereas the hydrogen bonds between Asp94 α , Arg95 α , Arg79, Asp80, and the hydroxyl groups on the sphingosine chain are maintained for all the analogs. As mentioned earlier, when either tyrosine is mutated into an alanine the binding affinity between TCR and CD1d drops significantly,⁵⁶ so that if either tyrosine cannot form hydrogen bonds to Glu83 then TCR cannot bind to CD1d. It is speculated that the reason for Arg103 α monopolizing the hydrogen bonding potential of Glu83 is due to the CDR3 α loop not being buried far enough into the binding cavity of CD1d. This is more apparent in the C2'-analogs rather than the C3'-analogs, where the C2' substituent is buried into the CD1d binding groove displacing the CDR3 α loop. It becomes even more apparent as the bulkiness of the substituent is increased as in 2'-NIV- α -GalCer (PGW306) (Figure 9J). Interestingly, the C4' aliphatic amide substituent, PGW508, maintains the tyrosine hydrogen bonding network; however, its bulkier counterpart the C4'

aromatic amide substituent, PGW408, did not implying that probably this glycolipid would not be an ideal candidate for iNKT stimulation (Figure 9K,L).

CONCLUSION

Molecular dynamics simulations provide an idea of how proteins behave in a solution environment. A reliable computational model was created where full box explicit solvation was found to reproduce most accurately the behavior of the tertiary complex. The lock-and-key interaction between TCR and CD1d was supported by rmsd calculations where a slight shift of TCR over the course of the simulation was attributed to the expected motion for this type of interaction. Furthermore, previous experimental mutation studies were correlated to an in-depth statistical and visual hydrogen bond analysis where it was found that Glu83 and Asp80 are the two most important residues on CD1d allowing for recognition and binding of TCR. The 49 glycolipid analogs were then docked into this computational model to yield a host of binding energies, where the binding

energy of α -GalCer to CD1d was comparable to the experimental binding energy providing some confidence in the accuracy and hence predictive nature of the other binding energies. The molecular dynamics simulations on selected glycolipids provided structural evidence for the difference in iNKT stimulation between the C2'-, C3'-, and C4'-substituted analogs where substitution at the C4'-position is more tolerated than at the C2'- and C3'-positions. Furthermore, the simulations predict that in order to accommodate the glycolipid sugar modification TCR must structurally change enough that a disruption of the hydrogen bond network occurs with primary emphasis on the tyrosines hydrogen bonding web.

The next important steps in understanding the recognition system of CD1d/glycolipid/TCR complex will be to create a hypothetical tertiary model of iGb3 based off the binding of β -GlcCer. Also, the binding energies of CD1d/glycolipid to TCR also need to be determined through protein–protein docking to develop a more accurate picture of the recognition process since this can be experimentally calculated and is the process on how a glycolipid is presented to CD1d. In conclusion, this study brings us a step closer in understanding the role that the sugar plays in the glycolipid, which will hopefully lead to the discovery of more potent analogs and maybe even the natural antigen for this system.

ACKNOWLEDGMENT

The Ohio Supercomputer Center (OSC) is acknowledged for their generous computational support of this research. The Ohio State University is also acknowledged for its support provided through the Ohio Eminent Scholar fund to Peng George Wang. Molecular graphics images were produced using the UCSF Chimera package⁶⁶ from the Resource for Biocomputing, Visualization, and Informatics at the University of California, San Francisco (supported by NIH P41 RR-01081).

Supporting Information Available: Graphs for all individual protein rmsd fluctuations calculated for the system, alignment images created from snapshots taken of the complexes along the simulation trajectory, a more extensive listing of the hydrogen bonding statistics from the simulations, and more extensive docking energy data of the glycolipid library. This material is available free of charge via the Internet at <http://pubs.acs.org>.

REFERENCES AND NOTES

- Krummel, M. F.; Davis, M. M. Dynamics of the immunological synapse: finding, establishing and solidifying a connection. *Curr. Opin. Immunol.* **2002**, *14*, 66–74.
- Bromley, S. K.; Burack, W. R.; Johnson, K. G.; Somersalo, K.; Sims, T. N.; Sumen, C.; Davis, M. M.; Shaw, A. S.; Allen, P. M.; Dustin, M. L. The immunological synapse. *Annu. Rev. Immunol.* **2001**, *19*, 375–396.
- Gao, G. F.; Jakobsen, B. K. Molecular interactions of coreceptor CD8 and MHC class I: the molecular basis for functional coordination with the T-cell receptor. *Immunol. Today* **2000**, *21*, 630–636.
- Van Kaer, L. α -Galactosylceramide therapy for autoimmune diseases: prospects and obstacles. *Nat. Rev. Immunol.* **2005**, *5*, 31–42.
- Gumperz, J. E. The ins and outs of CD1 molecules: bringing lipids under immunological surveillance. *Traffic* **2006**, *7*, 2–13.
- Gadola, S. D.; Dulphy, N.; Salio, M.; Cerundolo, V. Va24-JaQ-independent, CD1d-restricted recognition of α -galactosylceramide by human CD4+ and CD8ab+ T lymphocytes. *J. Immunol.* **2002**, *168*, 5514–5520.
- Martin, L. H.; Calabi, F.; Lefebvre, F. A.; Bilsland, C. A. G.; Milstein, C. Structure and expression of the human thymocyte antigens CD1a, CD1b, and CD1c. *Proc. Natl. Acad. Sci. U.S.A.* **1987**, *84*, 9189–9193.
- Martin, L. H.; Calabi, F.; Milstein, C. Isolation of CD1 genes: a family of major histocompatibility complex-related differentiation antigens. *Proc. Natl. Acad. Sci. U.S.A.* **1986**, *83*, 9154–9158.
- Calabi, F.; Milstein, C. A novel family of human major histocompatibility complex-related genes not mapping to chromosome 6. *Nature* **1986**, *323*, 540–543.
- Calabi, F.; Jarvis, J. M.; Martin, L.; Milstein, C. Two classes of CD1 genes. *Eur. J. Immunol.* **1989**, *19*, 285–292.
- Porcelli, S. A.; Modlin, R. L. The CD1 system: Antigen-presenting molecules for T cell recognition of lipids and glycolipids. *Annu. Rev. Immunol.* **1999**, *17*, 297–329.
- Brossay, L.; Chioda, M.; Burdin, N.; Koezuka, Y.; Casorati, G.; Dellabona, P.; Kronenberg, M. CD1d-mediated recognition of an α -galactosylceramide by natural killer T cells is highly conserved through mammalian evolution. *J. Exp. Med.* **1998**, *188*, 1521–1528.
- Parekh, V. V.; Wilson, M. T.; Van Kaer, L. iNKT-cell responses to glycolipids. *Crit. Rev. Immunol.* **2005**, *25*, 183–213.
- Kronenberg, M.; Gapin, L. The unconventional lifestyle of NKT Cells. *Nat. Rev. Immunol.* **2002**, *2*, 557–568.
- Natori, T.; Koezuka, Y.; Higa, T. Agelasphins, novel α -galactosylceramides from the marine sponge Agelas mauritanus. *Tetrahedron Lett.* **1993**, *34*, 5591–5592.
- Natori, T.; Morita, M.; Akimoto, K.; Koezuka, Y. Agelasphins, novel antitumor and immunostimulatory cerebrosides from the marine sponge Agelas mauritanus. *Tetrahedron* **1994**, *50*, 2771–2784.
- Morita, M.; Motoki, K.; Akimoto, K.; Natori, T.; Sakai, T.; Sawa, E.; Yamaji, K.; Koezuka, Y.; Kobayashi, E.; Fukushima, H. Structure-Activity Relationship of α -Galactosylceramides against B16-Bearing Mice. *J. Med. Chem.* **1995**, *38*, 2176–2187.
- Kobayashi, E.; Motoki, K.; Uchida, T.; Fukushima, H.; Koezuka, Y. KRN7000, a novel immunomodulator, and its antitumor activities. *Oncol. Res.* **1995**, *7*, 529–534.
- Shimosaka, A. Role of NKT cells and alpha-galactosyl ceramide. *Int. J. Hematol.* **2002**, *76* (Suppl 1), 277–279.
- Naumov, Y. N.; Bahjat, K. S.; Gausling, R.; Abraham, R.; Exley, M. A.; Koezuka, Y.; Balk, S. B.; Strominger, J. L.; Clare-Salzer, M.; Wilson, S. B. Activation of CD1d-restricted T cells protects NOD mice from developing diabetes by regulating dendritic cell subsets. *Proc. Natl. Acad. Sci. U.S.A.* **2001**, *98*, 13838–13843.
- Taniguchi, M.; Seino, K.-i.; Nakayama, T. The NKT cell system: bridging innate and acquired immunity. *Nat. Immunol.* **2003**, *4*, 1164–1165.
- Fujio, M.; Wu, D.; Garcia-Navarro, R.; Ho, D. D.; Tsuji, M.; Wong, C.-H. Structure-Based Discovery of Glycolipids for CD1d-Mediated NKT Cell Activation: Tuning the Adjuvant versus Immunosuppression Activity. *J. Am. Chem. Soc.* **2006**, *128*, 9022–9023.
- Miyamoto, K.; Miyake, S.; Yamamura, T. A synthetic glycolipid prevents autoimmune encephalomyelitis by inducing TH2 bias of natural killer T cells. *Nature* **2001**, *413*, 531–534.
- Yu, K. O. A.; Im, J. S.; Molano, A.; Dutranc, Y.; Illarionov, P. A.; Forestier, C.; Fujiwara, N.; Arias, I.; Miyake, S.; Yamamura, T.; Chang, Y.-T.; Besra, G. S.; Porcelli, S. A. Modulation of CD1d-restricted NKT cell responses by using N-acyl variants of α -galactosylceramides. *Proc. Natl. Acad. Sci. U.S.A.* **2005**, *102*, 3383–3388.
- Corver, J.; Moesby, L.; Erkullala, R. K.; Reddy, K. C.; Bittman, R.; Wilschut, J. Sphingolipid-dependent fusion of Semliki Forest virus with cholesterol-containing liposomes requires both the 3-hydroxyl group and the double bond of the sphingolipid backbone. *J. Virol.* **1995**, *69*, 3220–3223.
- Lang, G. A.; Maltsev, S. D.; Besra, G. S.; Lang, M. L. Presentation of α -galactosylceramide by murine CD1d to natural killer T cells is facilitated by plasma membrane glycolipid rafts. *Immunology* **2004**, *112*, 386–396.
- Rauch, J.; Gumperz, J.; Robinson, C.; Skoeld, M.; Roy, C.; Young, D. C.; Lafleur, M.; Moody, D. B.; Brenner, M. B.; Costello, C. E.; Behar, S. M. Structural Features of the Acyl Chain Determine Self-phospholipid Antigen Recognition by a CD1d-restricted Invariant NKT (iNKT) Cell. *J. Biol. Chem.* **2003**, *278*, 47508–47515.
- Zajonc, D. M.; Maricic, I.; Wu, D.; Halder, R.; Roy, K.; Wong, C.-H.; Kumar, V.; Wilson, I. A. Structural basis for CD1d presentation of a sulfatide derived from myelin and its implications for autoimmunity. *J. Exp. Med.* **2005**, *202*, 1517–1526.
- Kawano, T.; Cui, J.; Koezuka, Y.; Toura, I.; Kaneko, Y.; Motoki, K.; Ueno, H.; Nakagawa, R.; Sato, H.; Kondo, E.; Koseki, H.; Taniguchi, M. CD1d-restricted and TCR-mediated activation of Va14 NKT cells by glycosylceramides. *Science* **1997**, *278*, 1626–1629.

- (30) Iijima, H.; Kimura, K.; Sakai, T.; Uchimura, A.; Shimizu, T.; Ueno, H.; Natori, T.; Koezuka, Y. Structure-activity relationship and conformational analysis of monoglycosylceramides on the syngeneic mixed leukocyte reaction. *Bioorg. Med. Chem.* **1998**, *6*, 1905–1910.
- (31) Zeng, Z. H.; Castano, A. R.; Segelke, B. W.; Stura, E. A.; Peterson, P. A.; Wilson, I. A. Crystal structure of mouse CD1: an MHC-like fold with a large hydrophobic binding groove. *Science* **1997**, *277*, 339–345.
- (32) Wu, D.; Xing, G.-W.; Poles, M. A.; Horowitz, A.; Kinjo, Y.; Sullivan, B.; Bodmer-Narkevitch, V.; Plettenburg, O.; Kronenberg, M.; Tsuji, M.; Ho, D. D.; Wong, C.-H. Bacterial glycolipids and analogs as antigens for CD1d-restricted NKT cells. *Proc. Natl. Acad. Sci. U.S.A.* **2005**, *102*, 1351–1356.
- (33) Saubermann, L. J.; Beck, P.; De Jong, Y. P.; Pitman, R. S.; Ryan, M. S.; Kim, H. S.; Exley, M.; Snapper, S.; Balk, S. P.; Hagen, S. J.; Kanuchi, O.; Motoki, K.; Sakai, T.; Terhorst, C.; Koezuka, Y.; Podolsky, D. K.; Blumberg, R. S. Activation of natural killer T cells by a-galactosylceramide in the presence of CD1d provides protection against colitis in mice. *Gastroenterology* **2000**, *119*, 119–128.
- (34) Zhou, X.-T.; Forestier, C.; Goff, R. D.; Li, C.; Teyton, L.; Bendelac, A.; Savage, P. B. Synthesis and NKT Cell Stimulating Properties of Fluorophore- and Biotin-Appended 6"-Amino-6"-deoxy-galactosylceramides. *Org. Lett.* **2002**, *4*, 1267–1270.
- (35) Prigozy, T. I.; Naidenko, O.; Qasba, P.; Elewaut, D.; Brossay, L.; Khurana, A.; Natori, T.; Koezuka, Y.; Kulkarni, A.; Kronenberg, M. Glycolipid antigen processing for presentation by CD1d molecules. *Science* **2001**, *291*, 664–667.
- (36) Zhou, D.; Mattner, J.; Cantu, C., III.; Schrantz, N.; Yin, N.; Gao, Y.; Sagiv, Y.; Hudspeth, K.; Wu, Y.-P.; Yamashita, T.; Teneberg, S.; Wang, D.; Proia Richard, L.; Levery Steven, B.; Savage Paul, B.; Teyton, L.; Bendelac, A. Lysosomal glycosphingolipid recognition by NKT cells. *Science* **2004**, *306*, 1786–1789.
- (37) Koch, M.; Stronge, V. S.; Shepherd, D.; Gadola, S. D.; Mathew, B.; Ritter, G.; Fersht, A. R.; Besra, G. S.; Schmidt, R. R.; Jones, E. Y.; Cerundolo, V. The crystal structure of human CD1d with and without a-galactosylceramide. *Nat. Immunol.* **2005**, *6*, 819–826.
- (38) Wu, D.; Zajonc, D. M.; Fujio, M.; Sullivan, B. A.; Kinjo, Y.; Kronenberg, M.; Wilson, I. A.; Wong, C. H. Design of natural killer T cell activators: structure and function of a microbial glycosphingolipid bound to mouse CD1d. *Proc. Natl. Acad. Sci. U.S.A.* **2006**, *103*, 3972–3977.
- (39) Zajonc, D. M.; Savage, P. B.; Bendelac, A.; Wilson, I. A.; Teyton, L. Crystal Structures of Mouse CD1d-iGb3 Complex and its Cognate Va14 T Cell Receptor Suggest a Model for Dual Recognition of Foreign and Self Glycolipids. *J. Mol. Biol.* **2008**, *377*, 1104–1116.
- (40) Gadola, S. D.; Koch, M.; Marles-Wright, J.; Lissin, N. M.; Shepherd, D.; Matulis, G.; Harlos, K.; Villiger, P. M.; Stuart, D. I.; Jakobsen, B. K.; Cerundolo, V.; Jones, E. Y. Structure and binding kinetics of three different human CD1d-a-galactosylceramide-specific T cell receptors. *J. Exp. Med.* **2006**, *203*, 699–710.
- (41) Kjer-Nielsen, L.; Borg, N. A.; Pellicci, D. G.; Beddoe, T.; Kostenko, L.; Clements, C. S.; Williamson, N. A.; Smyth, M. J.; Besra, G. S.; Reid, H. H.; Bharadwaj, M.; Godfrey, D. I.; Rossjohn, J.; McCluskey, J. A structural basis for selection and cross-species reactivity of the semi-invariant NKT cell receptor in CD1d/glycolipid recognition. *J. Exp. Med.* **2006**, *203*, 661–673.
- (42) Borg, N. A.; Wun, K. S.; Kjer-Nielsen, L.; Wilce, M. C. J.; Pellicci, D. G.; Koh, R.; Besra, G. S.; Bharadwaj, M.; Godfrey, D. I.; McCluskey, J.; Rossjohn, J. CD1d-lipid-antigen recognition by the semi-invariant NKT cell receptor. *Nature* **2007**, *448*, 44–49.
- (43) Pearlman, D. A.; Case, D. A.; Caldwell, J. W.; Ross, W. S.; Cheatham, T. E., III.; DeBolt, S.; Ferguson, D.; Seibel, G.; Kollman, P. "AMBER", a package of computer programs for applying molecular mechanics, normal mode analysis, molecular dynamics and free energy calculations to stimulate the structural and energetic properties of molecules. *Comput. Phys. Commun.* **1995**, *91*, 1–42.
- (44) Morris, G. M.; Goodsell, D. S.; Halliday, R. S.; Huey, R.; Hart, W. E.; Belew, R. K.; Olson, A. J. Automated docking using a Lamarckian genetic algorithm and an empirical binding free energy function. *J. Comput. Chem.* **1998**, *19*, 1639–1662.
- (45) Bernstein, F. C.; Koetzle, T. F.; Williams, G. J. B.; Meyer, E. F., Jr.; Brice, M. D.; Rodgers, J. R.; Kennard, O.; Shimanouchi, T.; Tasumi, M. The Protein Data Bank: a computer-based archival file for macromolecular structures. *J. Mol. Biol.* **1977**, *112*, 535–542.
- (46) Jorgensen, W. L.; Chandrasekhar, J.; Madura, J. D.; Impey, R. W.; Klein, M. L. Comparison of simple potential functions for simulating liquid water. *J. Chem. Phys.* **1983**, *79*, 926–935.
- (47) Pellegrini, E.; Field, M. J. A Generalized-Born Solvation Model for Macromolecular Hybrid-Potential Calculations. *J. Phys. Chem. A* **2002**, *106*, 1316–1326.
- (48) Duan, Y.; Wu, C.; Chowdhury, S.; Lee, M. C.; Xiong, G.; Zhang, W.; Yang, R.; Cieplak, P.; Luo, R.; Lee, T.; Caldwell, J.; Wang, J.; Kollman, P. A point-charge force field for molecular mechanics simulations of proteins based on condensed-phase quantum mechanical calculations. *J. Comput. Chem.* **2003**, *24*, 1999–2012.
- (49) Woods, R. J.; Dwek, R. A.; Edge, C. J.; Fraser-Reid, B. Molecular Mechanical and Molecular Dynamic Simulations of Glycoproteins and Oligosaccharides. 1. GLYCÁM_93 Parameter Development. *J. Phys. Chem.* **1995**, *99*, 3832–3846.
- (50) Wang, J.; Wang, W.; Kollman, P. A.; Case, D. A. Automatic atom type and bond type perception in molecular mechanical calculations. *J. Mol. Graphics Modell.* **2006**, *25*, 247–260.
- (51) Wang, J.; Wolf, R. M.; Caldwell, J. W.; Kollman, P. A.; Case, D. A. Development and testing of a general Amber force field. *J. Comput. Chem.* **2004**, *25*, 1157–1174.
- (52) MacroModel, version 8.5; Schrödinger Inc.: Portland, OR, 2003.
- (53) Still, W. C.; Tempczyk, A.; Hawley, R. C.; Hendrickson, T. Semi-analytical treatment of solvation for molecular mechanics and dynamics. *J. Am. Chem. Soc.* **1990**, *112*, 6127–6129.
- (54) Jorgensen, W. L.; Tirado-Rives, J. The OPLS [optimized potentials for liquid simulations] potential functions for proteins, energy minimizations for crystals of cyclic peptides and crambin. *J. Am. Chem. Soc.* **1988**, *110*, 1657–1666.
- (55) Guex, N.; Peitsch, M. C. SWISS-MODEL and the Swiss-PdbViewer. An environment for comparative protein modeling. *Electrophoresis* **1997**, *18*, 2714–2723.
- (56) Wun, K. S.; Borg, N. A.; Kjer-Nielsen, L.; Beddoe, T.; Koh, R.; Richardson, S. K.; Thakur, M.; Howell, A. R.; Scott-Browne, J. P.; Gapin, L.; Godfrey, D. I.; McCluskey, J.; Rossjohn, J. A minimal binding footprint on CD1d-glycolipid is a basis for selection of the unique human NKT TCR. *J. Exp. Med.* **2008**, *209*, 939–949.
- (57) Savage, P. B.; Teyton, L.; Bendelac, A. Glycolipids for natural killer T cells. *Chem. Soc. Rev.* **2006**, *35*, 771–779.
- (58) Sakai, T.; Naidenko, O. V.; Iijima, H.; Kronenberg, M.; Koezuka, Y. Syntheses of Biotinylated a-Galactosylceramides and Their Effects on the Immune System and CD1 Molecules. *J. Med. Chem.* **1999**, *42*, 1836–1841.
- (59) Kawano, T.; Cui, J.; Koezuka, Y.; Toura, I.; Kaneko, Y.; Motoki, K.; Ueno, H.; Nakagawa, R.; Sato, H.; Kondo, E.; Koseki, H.; Taniguchi, M. CD1d-restricted and TCR-mediated activation of valpha14 NKT cells by glycosylceramides. *Science* **1997**, *278*, 1626–1629.
- (60) Kinjo, Y.; Wu, D.; Kim, G.; Xing, G.-W.; Poles, M. A.; Ho, D. D.; Tsuji, M.; Kawahara, K.; Wong, C.-H.; Kronenberg, M. Recognition of bacterial glycosphingolipids by natural killer T cells. *Nature* **2005**, *434*, 520–525.
- (61) Cantu, C., III.; Benlagha, K.; Savage, P. B.; Bendelac, A.; Teyton, L. The Paradox of Immune Molecular Recognition of a-Galactosylceramide: Low Affinity, Low Specificity for CD1d, High Affinity for ab TCRs. *J. Immunol.* **2003**, *170*, 4673–4682.
- (62) Sidobre, S.; Hammond, K. J. L.; Benazet-Sidobre, L.; Maltsev, S. D.; Richardson, S. K.; Ndonye, R. M.; Howell, A. R.; Sakai, T.; Besra, G. S.; Porcelli, S. A.; Kronenberg, M. The T cell antigen receptor expressed by Va14i NKT cells has a unique mode of glycosphingolipid antigen recognition. *Proc. Natl. Acad. Sci. U.S.A.* **2004**, *101*, 12254–12259.
- (63) Ortaldo, J. R.; Young, H. A.; Winkler-Pickett, R. T.; Bere, E. W., Jr.; Murphy, W. J.; Wiltz, R. H. Dissociation of NKT Stimulation, Cytokine Induction, and NK Activation In Vivo by the Use of Distinct TCR-Binding Ceramides. *J. Immunol.* **2004**, *172*, 943–953.
- (64) Stanic, A. K.; De Silva, A. D.; Park, J.-J.; Sriram, V.; Ichikawa, S.; Hirabayashi, Y.; Hayakawa, K.; Van Kaer, L.; Brutkiewicz, R. R.; Joyce, S. Defective presentation of the CD1d1-restricted natural Va14Ja18 NKT lymphocyte antigen caused by b-D-glucosylceramide synthase deficiency. *Proc. Natl. Acad. Sci. U.S.A.* **2003**, *100*, 1849–1854.
- (65) Long, X.; Deng, S.; Mattner, J.; Zang, Z.; Zhou, D.; McNary, N.; Goff, R. D.; Teyton, L.; Bendelac, A.; Savage, P. B. Synthesis and evaluation of stimulatory properties of Sphingomonadaceae glycolipids. *Nat. Chem. Biol.* **2007**, *3*, 559–564.
- (66) Pettersen, E. F.; Goddard, T. D.; Huang, C. C.; Couch, G. S.; Greenblatt, D. M.; Meng, E. C.; Ferrin, T. E. UCSF Chimera-A visualization system for exploratory research and analysis. *J. Comput. Chem.* **2004**, *25*, 1605–1612.